A Novel Approach to Shape Memory Alloys Applied to Passive Adaptive Shading Systems

Lorenzo Vercesi[1,2], Alberto Speroni[1*], Andrea Giovanni Mainini[1], Tiziana Poli[1]

* Corresponding author
1 Department of Architecture, Built Environment and Construction Engineering, Politecnico di Milano, Italy, alberto.speroni@polimi.it
2 Buro Happold, London, United Kingdom

Abstract

A shading device for façade application was developed by combining twisting cylindrical shading elements with the smart use of shape-memory alloy (SMA) components. These allow a dynamic behaviour of a shading device, which does not require electrical motors or manual activation, nor sophisticated electronic controls. The technical development of the system involved research of cylindrical shading geometries, which can transition from straight to hourglass configuration, given a 180° rotation, with limited mechanical movement. This is induced by the stroke of a SMA spring, which functions as both actuator and sensor. Its design is tailored to achieve a passive adaptive component that can be activated under set temperature stimuli, caused by incident solar radiation on a façade. A combination of computer simulations and physical tests were carried out to assess the optimal conditions of the SMA spring activation in a temperate climate condition (Cfa to the Koppen-Geiger classification), correlating transition temperature (50°C), incident solar radiation (>300W/m^2) and the forces required to operate the cylinders. In parallel, an experimental apparatus was developed to validate the concept on a geometrical point of view, and to ensure its constraints were compatible with a SMA spring control system.

Keywords

Passive adaptive, shading system, shading device, dynamic, innovative, double-skin, shape memory alloy springs, solar radiation, daylight

DOI 10.7480/jfde.2020.1.4700

1 INTRODUCTION

Nowadays, building envelopes are assuming a new identity: a gradual reduction in the solid area of the façade in favour of transparent surfaces is in vogue in the context of contemporary architecture. The continuous evolution of the glazing system is not always sufficient to guarantee a dynamic behaviour that ensures users' comfort and optimal energy consumption (e.g. for cooling). Therefore, curtain walling is being progressively coupled with dynamic solar protection. An efficient solar shading system can reduce overheating in commercial buildings by about 10% to 20% (this value can change depending on several parameters such as climate, transparent surface percentage, building morphology, and shading type) (Menzies & Wherrett, 2005; Palmero-Marrero & Oliveira, 2010; Tzempelikos & Athienitis, 2007). The reduction of solar gains for fixed shading devices system is usually associated with a reduction in natural daylighting, resulting in an increase of energy consumption due to artificial lighting (Heschong, 2002). Alternatively, dynamic shading devices allow different configurations in order to respond to users' needs. In their simplest configuration, these systems can be controlled directly by the users; however, this manual mode is not efficient, since users are required to change the shading devices position periodically. The worst possible scenario results in the device being set at an extreme position permanently (i.e. completely closed or open), thus turning the system into a static solution (Wang, Pichatwatana, Roaf, Zhao, Zhu, & Li, 2014; Nielsen, Svendsen, & Jensen, 2011). A second type of dynamic shading is an automated one, where the configuration of shading devices is controlled automatically depending on environmental factors. Energy optimisation of this solution could be achieved by sensors and actuators, which can be part of the shading device or can be delocalised: sensors allow the collection of precise and localised information about physical parameters; actuators provide a dynamic response based on these parameters. The dynamic actuation is possible thanks to motors and mechanical transmission elements, through which it is possible to control multiple shading elements, in turn making the overall system more cost effective. The main issues for a dynamic shading system are a lower comfort level for users due to a diffused shading actuation, and a high risk of failure due to a wide use of mechanical parts.

The integration of smart materials (SMs) within shading systems enables an adaptive behaviour of the device and, depending on the intensity of solar radiation, reduces the system's complexity by avoiding the use of motorised mechanical parts. Direct consequences are reduced energy consumption and lower risk of failure. Fiorito et al. (2016) presented a detailed analysis of the actuation possibilities of shading systems by comparing their performances and working principles. The results highlight that SMs show the ability "to possess the characteristics to work as actuators either separated or integrated into shading components" (Fiorito et al., 2016). Within the realm of SMs, those that have been identified as suitable for this purpose, due to their durability and surety of performance, are shape memory alloys (SMAs) for the forces produced during their phase-change transition and their durability (high number of hysteresis cycle under certain condition). Like many other smart materials, SMAs require a tailor-made new shading functional model based on their material properties, which can be customised depending on the application.

A new shading device, which can change its configuration based on a passive adaptive approach, as defined by Mazzucchelli, Romano, Aelenei, and Gomes (2018), has been developed using SMA springs. These springs function as both sensor and actuator, and they change the configuration of the shading device (geometry, orientation, etc), avoiding phenomena such as overheating and glare.

The objective of this research study was to assess the mechanical and geometrical limitations of SMA springs, and to develop an innovative shading geometry that was compatible with these specific

design constraints (climate, activation criteria) defined in Chapter 3.1. Once the initial parameters had been defined, simulations and physical experiments were carried out on a number of design options (including system configuration, orientation, time over a day and a year) to correlate input stimuli on a vertical façade (incident solar radiation) with passive adaptive activation for a shading device, thus determining the range of application as a dynamic shading system.

1.1 BACKGROUND

Shape memory alloys (SMAs) are materials typically used in the medical and automotive sector for their reliability and integrability, as actuator or sensor. SMAs can be shaped with many geometries but their typical form is the helicoidal spring and simple wires since these geometries maximise the feature of the memory shape alloy. SMAs can be activated by temperature or electricity (via Joule effect), making them suitable for both active and passive adaptive solutions. Several shading concepts found in current literature use SMAs with different approaches. Table 1 presents different examples of SMA-based shading systems, categorised by estimated Technology Readiness Level (TRL), and by type of control and activation.

TABLE 1 SMA-Based Shading Systems. (*Technology Readiness Level (TRL) estimated by the authors based on the information available on literature and online).

N°	SHADING SYSTEM	LITERATURE REFERENCE	SMA GEOM-ETRY	ESTIMATED TRL*	TYPE CONTROL	ACTIVATION STIMULUS
A1	Self-Adaptive Membrane	Decker & Yeadon, 2006	Spring	4-5	Diffuse	Temperature
A2	ADAPTIVE[SKINS]	Gonzalez, 2015	Spring	2-3	Diffuse	Temperature
A3	SmartScreen (Version C)	Luna, 2014	Spring	3-4	Diffuse	Temperature
A4	Shape Memory Alloy Responsive Façade	Adaptive Skin, 2015	Spring	3-4	Diffuse	Temperature
B1	Gill_Project	Sandoval, 2012	Wire	3-4	Local	Electrical
B2	Shutters A Permeable Surface	Coelho & Zigelbaum, 2011	Wire	2-3	Local	Electrical
B3	THE AIR FLOW(ER)	L.Architects, 2008	Wire	2-3	Local	Electrical
B4	Pixel Skin	Pixel Skin, 2006	Wire	4-5	Diffuse	Electrical

1.1.1 Spring-Based devices

"SmartScreen – Version C" (Decker & Yeadon, 2006), (Figure 1-A1) consists of two sliding screens, both of which comprise alternating opaque and transparent horizontal stripes. Such stripes vary their permeability by means of the shifting of the two sheets and overlapping of stripes, giving a solar permeability with an openness factor range of 50 to 100%. The control is a diffused passive type and consists of two springs (SMA r-type + standard bias) with indoor positioning. "Self-adaptive membrane" (Gonzalez, 2015), (Figure 1-A2) consists of an architectural skin with integrated passive adaptive actuators made by SMA with bias spring integrated into a transparent cylinder. The actuators change the shape of the skin locally, which increases its thickness with a low variation in its openness factor. Compared to the previous system, it is characterised by a higher number of control points that are connected in a single skin, which results in a less adaptive solution. "SMA

responsive skin" (Luna, 2014), (Figure 1-A3) consists of a single small module activated passively by a SMA spring. These modules have a central hole connected to a central axis. This axis is connected to the SMA spring that changes its shape by turning the axis, and consequently changing the openness factor of the system. "Adaptive skin" (Adaptive Skin, 2015), (Figure 1-A4) is a flexible shading material connected directly to SMA and bias springs. It is an architectural skin, therefore the variation in the position of a single module has consequences that affect the entire skin. Compared to the previous presented system, it is characterised by three SMA springs per element, which increases the possibility of control but also increases complexity and costs.

1.1.2 Wire-based Devices

The second type of geometry used for the SMA is the wire. The first two systems presented are "the air flower" (L.Architects, 2008), (Figure 1-B1) and "Pixel skin" (Pixel Skin, 2006), (Figure 1-B2). Both systems consist of a square element with four rigid adjustable flaps that can open/close passively, turning around the frame on the perimeter. The first of the two integrates the wire in the frame while the second one integrates the wire in the shading element.

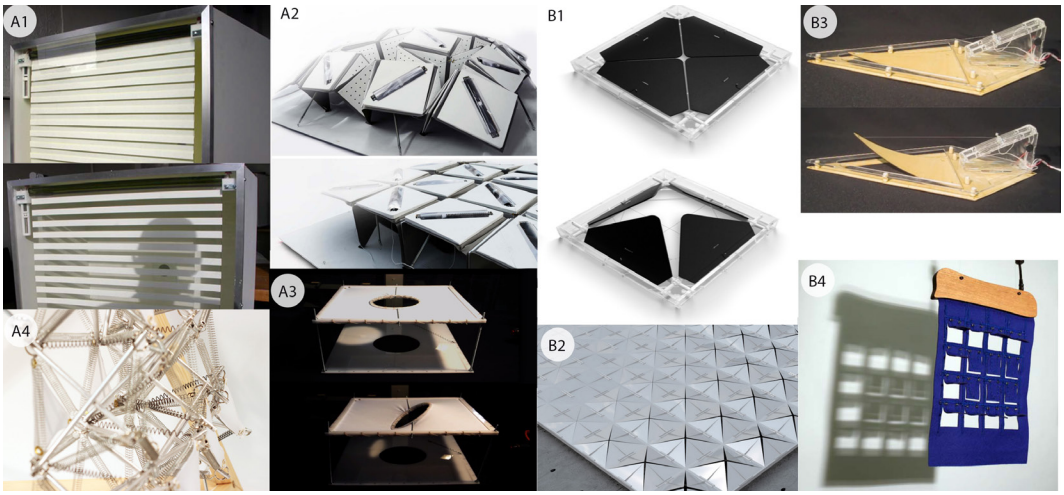

FIG. 1 [A1] SmartScreen - Version C (M. Decker, P. Yeadon). [A2] Self-Adaptive Membrane (N. Gonzales, S. More). [A3] Shape Memory Alloy Responsive Façade (I. Luna, M. Belge). [A4] ADAPTIVE[SKINS] (RatLab). [B1] THE AIR FLOW(ER) (Lift Architects). [B2] Pixel Skin (Orangevoid). [B3] Gill_Project (J. Sandoval). [B4] Shutters A Permeable Surface (M. Coelho)

"The Gill Project" (Sandoval, 2012), (Figure 1-B3) consists of a rhomboidal opaque element that can move thanks to a SMA wire connected to the fixed part that is activated by current. This active approach allows a higher possibility of control, even if the variation of the openness factor is low. "Shutters: a permeable surface" (Coelho & Zigelbaum, 2011; Coehlo & Maes, 2009), (Figure 1-B4) consists of a flexible opaque material that can change its openness factor thanks to the SMA integrated wire. The moveable shutters can assume all desired patterns, and their opening can be managed singularly. This allows the creation of many activation patterns in response to the users' requirements.

1.1.3 Systems Comparison

Fig. 2 presents a flexibility analysis of the shading control previously presented. By comparing the delta openness factor (variation in the percentage of the area between open and closed position) with the number of control activation points (modules per square metre), it is possible to identify the target design area with the optimum condition (high delta openness factor and high number of control points) of shading possibility and system user adaptability.

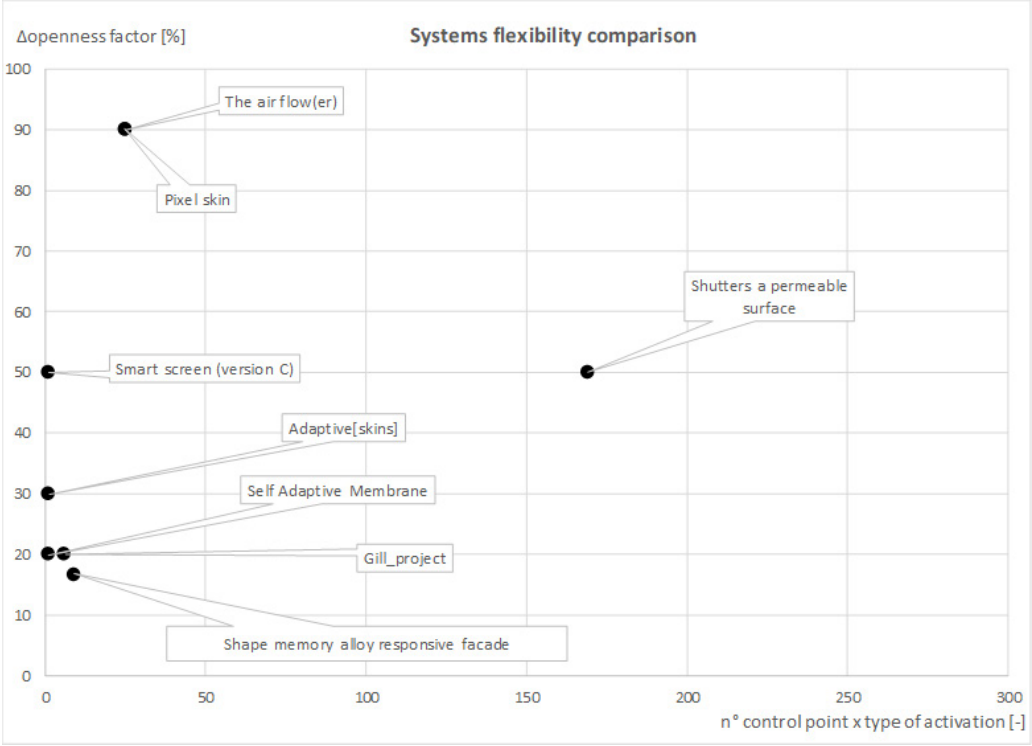

FIG. 2 Smart Shading Systems flexibility comparison

2 METHODOLOGY

2.1 SYSTEM DEVELOPMENT AND OPERATING PRINCIPLES

The shading system proposed is based on SMA springs that are activated passively.
The implementation of a customised working principle allowed the optimisation of the alloy features and consequently of the shading system performance.

Fig. 3 presents the approach followed in order to design the shading system: the definition of the working principles and technology allowed to identify the preliminary information for daylighting properties, and therefore for daylighting simulations. Meanwhile, the technology has been

continuously developed in order to optimise the alloy properties, making it more effective, with a detailed analysis of the moveable parts and their prototyping.

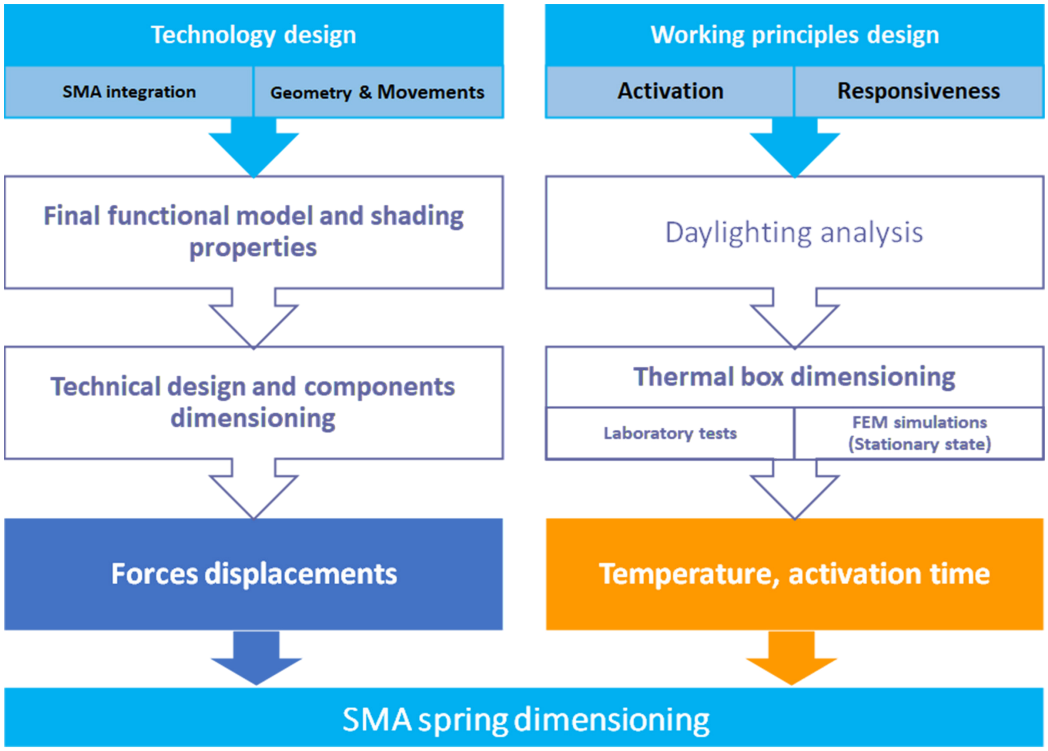

FIG. 3 Design approach description

2.1.1 Form Finding

The design flow started with the analysis of a cylindrical surface with top and bottom sides, which can rotate relative to each other, and the longitudinal fibres shaped around the lateral surface constrained to follow the rotation (and thus to twist). Such cylinders can be arranged parallel or orthogonal to the façade plane, and the rotation of one of the two sides (bottom or top) allows the shrinkage/elongation of the lateral surface to vary the openness factor of the shading system.

The considered arrangement was equal to a double-layer fabric. In fact, when the shadings are in the closed position and the cylinders are fully deployed, a mutual shading effect happens due to the overlap between the vertical fibres on the front and the backside of the cylinders.

A shading or privacy device comprising multiple cylinders with an axis orthogonal to the façade plane (Fig. 4, left) would allow for the local variation of the visual area, giving maximum flexibility to the users, and creating an efficient multi-zoning of the façade area: this effect, which resembles the behaviour of analogic camera shutters, could be exploited to provide effective shading to a façade, or to create visual transparency only in those areas where it is required. However, the geometrical constraints given by the thickness (height) of the cylinders, the required elongation ratio of the fibres

comprising the surface of the cylinders, along with the relationship between twisting rotation and variation of visual area, were found to pose significant challenges in the development of this system.

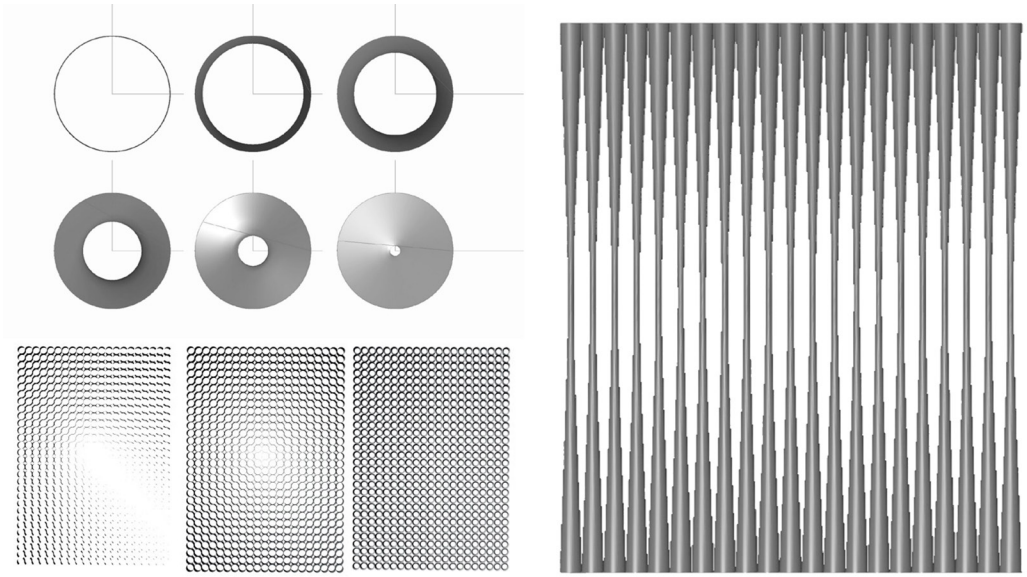

FIG. 4 [left] Cylinder's Hortogonal arrangement alternative [right] Cylinder's Vertical arrangement alternative

In order to complete a full transition from transparent to fully opaque, the cylinders need to make a full 180-degree rotation, which with such proportions (e.g. with height equal to the diameter) would result in extreme elongation ratios. This magnitude of movement would be challenging to achieve with a variety of materials, and to be maintained over time, due to phenomena such as metal fatigue or creep (for polymers). To mitigate this phenomenon, cylinders would need to be taller; however, in the context of façade application, this goes against the principle of a compact façade build-up, and negates certain applications, such as inclusion within cavities of insulated glazed units. Finally, automation, transmission, and coordination of movements across an array of cylinders would be challenging, requiring several components to be connected across a single façade module: as the cylinders are perpendicular to the façade, those links or transmissions would be in sight, making a concealed mechanism harder to achieve.

Having observed the challenges of "square" cylinders, and the benefit in divorcing from small height-to-diameter ratios, slender cylinders were explored, specifically with a parallel arrangement compared to the façade (Fig. 4, right). It was found that, whilst slender cylinders limit the degree of control over the façade transparency, they require a much simpler mechanical system compared to short cylinders. A more extreme aspect ratio would also mean a much lower percentage of elongation of the fibres which, depending on the material of such elements, would also result in lower tension forces. With vertical cylinders, the variation from open to closed position places the transition zone (from open to closed) in the central part of the façade vision area, which is typically at head height on a full-height façade module; the rotating parts, instead, may be placed at the top and bottom of the panel, therefore sitting within the peripheral zone of the façade module. This allows the mechanical parts to be concealed in the panel's perimeter frame, enabling activation of multiple cylinders with a single actuator, hence reducing the complexity of the system.

Given the benefit of slender cylinders with the axis parallel to the façade plane, this solution was pursued; square, orthogonal cylinders were disregarded as they were deemed not viable in the context of mechanisation into a shading device. The slender cylinders were subject to a thorough system development process, which involved further optimisation to enhance their reliability and efficiency (Fig. 5).

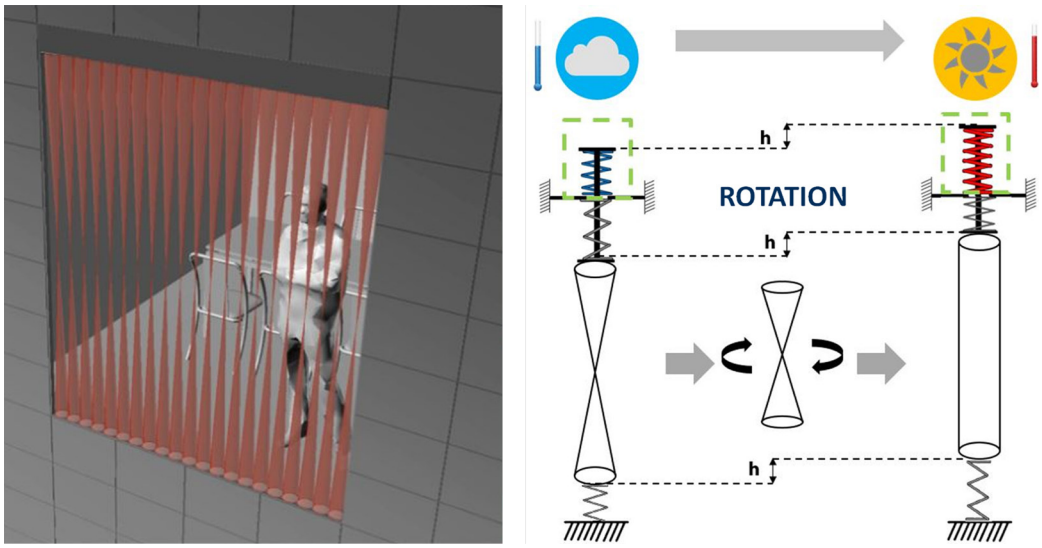

FIG. 5 [Left] System conceptual appearance. [right] Functional Model

2.1.2 Components Breakdown

This system comprises two main components:

- The thermal control box, where the SMA spring is placed;
- The twisting cylinders, which are the shading component of the system

The thermal box is the thermo-responsive environment, where the SMA component (in this case a spring) is thermally stressed by environmental stimuli (i.e. heat derived from incident solar radiation). As the SMA spring reaches the activation temperature, the shape memory effect takes place, modifying the shear modulus G, causing the tensile/compressive force of the spring to activate the shading device. With the solar radiation falling below a predefined threshold, the temperature progressively decreases, and the spring (coupled with the bias element) drives the system back to its initial configuration. Because of the inherent thermal inertia of the system, the deactivation temperature is not equal to the activation temperature, as the whole cycle is subject to a hysteresis phenomenon.

The key to unlocking the potential of this system is to calibrate the SMA activation temperature to match the activation (and deactivation) temperature for the system of the desired application. This can be done, to a limited extent, by choosing a SMA component with suitable chemical composition, since different SM alloys are characterised by different austenitic start temperatures. The optimal activation temperature, on the other hand, will depend on a number of factors, such as the context of

application (solar orientation, climate, wind exposure, etc.), mode of activation (by solar radiation or by Joule effect with electrical current) and the overall thermal inertia of the system (insulation of the thermal box, colour, etc.).

The twisting cylinders are the visible part of the system that can have variable height and diameter depending on the requirement. These elements are characterised by two different configurations:

- "Closed": when the top connection of the cylinder is up, the lateral surface of the cylinder is straight, and the entire visual area is shaded; this occurs when the SMA spring is above the switching temperature (activated);
- "Open": when the top connection of the cylinder is down, the lateral surface of the cylinder has an hourglass shape. The visual open area is approximately 50%, and it is localised in the centre of a full-height glazing system, thus maximising views to the outside, which can enhance comfort parameters. This occurs when the SMA spring is below the switching temperature (not activated)

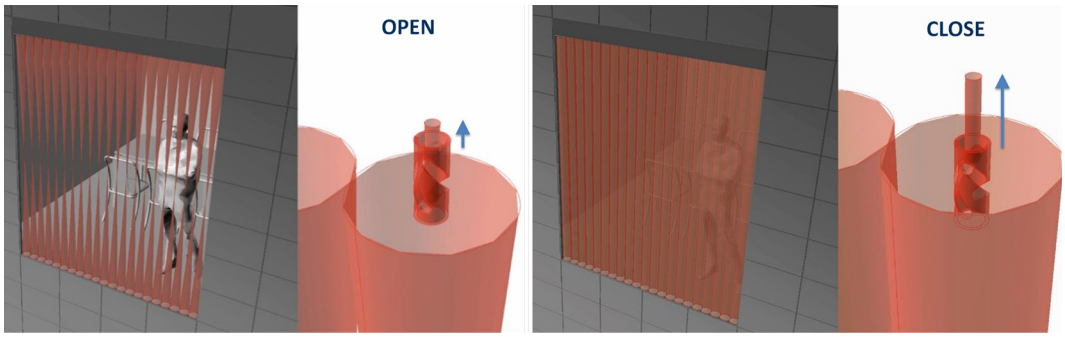

FIG. 6 System conceptual appearance in open and closed state. Focus on the axle movement

The twisting cylinders consist of three parts: top connection, shading element, and bottom connection. The top connection design is a critical part that integrates different components:

- A disk (Fig. 7, Detail 11), from which the shading component is hung, with a particular edge shape in order to fix the fabric/cords, and a tapered hollow cylinder (Fig. 7, Detail 12) in the middle with two opposite semi-helical slots that extend vertically as long as the stroke of the spring and 180° from edge to edge around the lateral surface of the tube. The inclination of the slots is designed to be 45°, so that the vertical pulling/compressing linear force can easily be transformed into a tangential force that generates a torque, thus giving rise to the rotation of the shading elements.
- An axle (Fig. 7, Detail 09) goes into the tapered hollow cylinder, and it has two horizontal pins on the external side that slide into the two semi-helical slots; the two cylinders slide one into the other, thus they are forced to relatively rotate. This axle is fixed to the upper frame from the bottom and, within this, we find the bias spring, which is a regular compressive spring capable of resetting the SMA spring as soon as the temperature drops below the activation temperature.
- A second hollow cylinder (Fig. 7, Detail 03) is fixed on the upper side of the fixed frame and contains the SMA compressive spring (Fig. 7, Detail 05), therefore it was designed to be the same length as the free length of the spring plus its typical (maximum) stroke. This cylinder has open lateral sides, to maximise heat exchange with the air contained inside the thermal box.

— An internal stick (Fig. 7, Detail 06) passes through the two springs and connects the top end of the SMA spring, which is a slider, with the bottom end of the tapered cylinder; therefore, when the SMA spring lifts the slider, the stick transmits the movement to the disk that goes up accordingly.

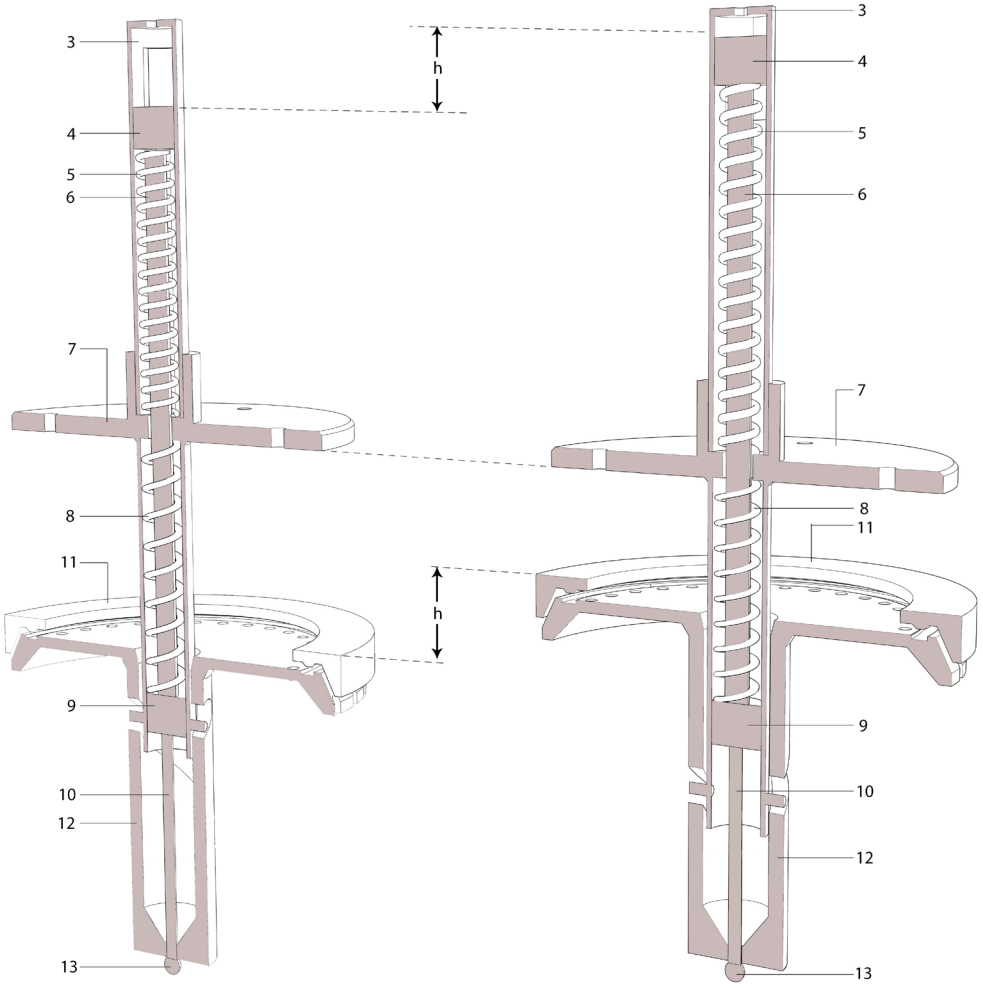

FIG. 7 The top connection Detail "Patent WP2018116102-A1"

The shading elements are the components that control solar radiation. The flexibility of the design system allows for the integration of different materials (textile, metal, plastic) with different geometry (strip, tube, cords, etc). Regarding the materiality of the cylinders, there are some restrictions on what concerns the geometry: cords and strips are better suited to accommodate the dynamic movement of the system, since they preserve a good appearance and do not ripple. This cannot be said for a continuous surface, such as a fabric: in fact, rippling can be observed in a fabric-type surface (by means of geometry modelling or even prototyping), when the cylinder transitions between its extreme states (cylinder and hourglass configuration), and this can be explained by purely comparing the surface area of the two configurations, which shrinks and causes the rippling phenomenon.

Fatigue (or creep) over repeated cycles would affect the durability of the system, which in turn would have an impact on maintenance requirements.

The bottom connection is the element that keeps the shading elements in tension. Depending on the material, this disk can be fixed or moveable. The moveable configuration consists of a vertical movement (no rotation allowed) and a bias element that guarantees adequate positioning of the shading elements. 3D-printed prototypes of both top and bottom connections have also been produced (refer to Fig.10, right).

2.2 SMA SPRING DEFINITION

The compatible sub-components of the mechanism were designed considering transmitted force and displacement. The assumption was that the longitudinal fibres of the fabric (or the cords themselves) are of fixed length: this means that the cord length is constant, whereas the height of the cylinders varies with the rotation. Considering the longitudinal fibres inextensible is in order to avoid stress relaxation and stretching in the fibre or cords, to make the component durable, However, in order to set a full 180-degree rotation, the hollow cylinder with semi-helical slots is designed with a larger displacement, since the displacement and the radius are related.

In Fig. 8 (left and centre) a diagram of the system is presented to understand the relation between forces and displacement subsequently discussed.

Therefore, considering a commercial compressive SMA spring, a good compromise between cost and effectiveness was obtained selecting a spring with an average diameter that can fit a hollow cylinder with a mean radius, r, equal to 9 mm. Fig. 8 (right) describes in a diagram the relationship between the angle β and the rate of change of the forces required and displacements obtained.

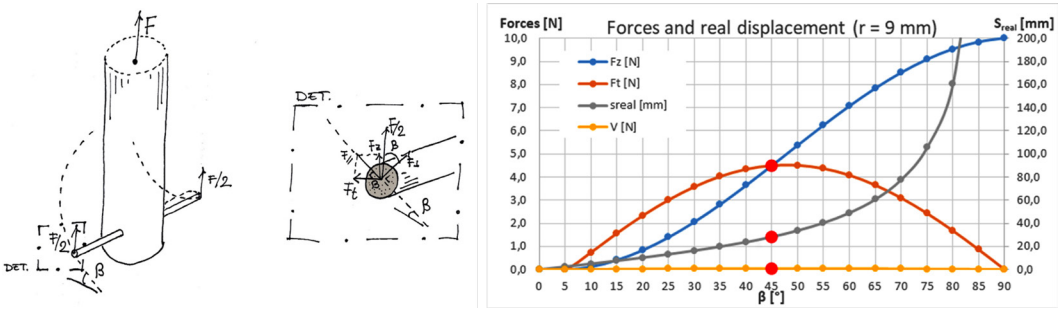

FIG. 8 Force, Displacements, and Temperatures of the compressive SMA spring. Tangential component of the forces (ft), tangential force (V), real displacement (sreal), Vertical component of the forces (Fz)

The force is transmitted through this component, and there is a precise rate between radius, spring pulling force and resultant vertical and torque force, due to friction and vectors components of forces. β is the slope angle used to split the forces over the axle in different tangential components, moreover, the higher the inclination of the slots (β), the more pulling force is transmitted from the

spring to the cylinder; however, the higher this angle, the higher the real displacement, so the stroke of the spring should be higher.

For a balance point of β=45° the selected compressive SMA spring is compliant with the requirement in terms of force and displacement only within a range between 50°C and 55°C.

3 SIMULATIONS AND EXPERIMENT

The design workflow for the thermal control box consisted of a first phase of solar and thermal analysis, which linked a range of activation temperatures to levels of incident solar radiation, with considerations given to frequency of activation and the responsiveness of the system over the course of a year. This phase was followed by physical testing, where a prototype was tested by measuring internal temperatures reached inside a thermal box subject to pre-defined radiation levels given by an artificial source.

3.1 SOLAR AND THERMAL ANALYSIS

The purpose of the solar and thermal analysis is to link temperatures reached inside the thermal box with incident solar radiation. Specifically, the aim of this analysis is to:

- Define the optimal activation temperature of the thermosensitive element (SMA Spring), contained inside the thermal box, which activates the transmission of the system and allows the movement of the shading element.
- Verify the frequency of occurrence of implementation in an annual application scenario, and to verify if the activation of the system is mainly due to combined optimal values of irradiance and external air temperature.
- Maximise the number of activation occurrences due to the incident solar radiation, and for the months (or hours) of the year, during which solar control is needed mainly to reduce primary energy for cooling (summer scenario), or to optimise daylighting (winter scenario).

Due to the significant number of variables (external temperatures, irradiance, wind, orientation, etc.), which govern the functioning of the thermal box, the solar and thermal analysis was carried out considering a specific case study, rather than a generalised scenario. The same workflow may be followed for other contexts. The selected case study comprised a thermal box located in Milan (Italy 45°28'38"28 N, 09°10'53"40 E), arranged in vertical position, and south-oriented. A realistic system was modelled, by defining a thermal box (with its own boundaries), as described in the previous paragraphs. The outer surfaces of the thermal box are thermally insulated with 3 cm of thermal insulation, except for the exposed face that consists of a glazed plane able to allow the passage of incident solar radiation. The internal surface of the thermal box, which directly receives the solar radiation, has an absorption coefficient of 0.9 and a low-emissivity value equal to 0.4. No mechanical ventilation is assumed within the box, but an infiltration rate equal to 1 ACH is considered, to allow for ventilation and imperfections in the sealing of the joints. The convective heat-exchange coefficients in the proximity of the external surfaces of the thermal box were calculated using the hourly average value of the wind speed for a north-to-south wind direction.

The summer discomfort variables considered as a reference scenario were an outdoor air temperature value of 25°C and an irradiance value on vertical surfaces of 300 W/m^2.

The SMA actuator is required to self-activate with direct solar radiation on the façade surface > 300 W/m^2. Whenever this value goes below this threshold, the transition temperature in the thermal box goes down accordingly and the shadings open up. For this assessment, the amount of time in one year (in hours, days, months) when the Incident solar radiation (ISR) on vertical surfaces is above 300 W/m^2 was calculated.

Fig. 9 shows a carpet plot of the annual distribution of the irradiance over the external surface of the thermal box. The vertical axis shows the hours in a day, whereas the horizontal axis shows the days and months over a year; the hours of the year when the air temperature is higher than 25°C are shown by means of regions bound by continuous black line.

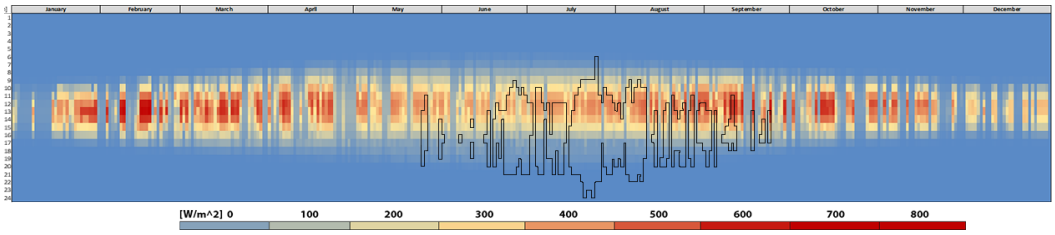

FIG. 9 Annual distribution of irradiance on a vertical unshaded surface facing south, for Milan (Italy), with hours on the vertical axis and days in one year on the horizontal axis

In reality, ISR values are probabilistic estimates, since they do not solely depend on sun path, but they are also influenced by weather conditions and urban context (mutual shadings due to geometry and context, building reflections, etc.). Milan (Italy) was considered as a case-study weather location for the test. ISR values on vertical surfaces were derived for the main orientations (east-south-west) and an in-depth analysis was done only for some representative days during the year. To predict the number of activation instances of the system, an assessment of the number of hours for each month in which ISR is above a fixed threshold (from 200 to 700 W/m^2) was carried out.

3.2 THERMAL BOX TEST AND EXPERIMENTAL SET-UP

The analysis presented in Chapter 3.1 formed the basis on which to predict the range of ISR on a vertical surface, as well as the variability of the related outside air temperature for a selected weather location.

Considering these boundary conditions, preliminary tests of the geometry and material properties of the thermal box were performed, using simulation FEM (Finite Elements Method) software: Physibel Voltra for 3D dynamic simulation; Physibel Bisco for 2D static simulation. The limit of static thermal analyses lies in its methodology, which presents results in stationary conditions, thus mainly highlighting the peak conditions that can be reached inside the thermal box; on the other hand, dynamic simulations gave an effective prediction of the time shift and delay in temperature increase

and decrease in accordance with ISR. The intermediate simulation steps, not presented in this paper, were useful to test different geometrical variants of the box, as well as the optical properties of the materials, or the expected insulation and air infiltration levels.

The analysis results were then processed, to inform the final characteristics of the responsive thermal environment (i.e. the thermal box) to host temperature-specific SMA components, with a defined austenitic start temperature (As).

Full-scale thermal box models (Fig. 10, left) were then created and tested under laboratory conditions, which were consistent with the boundary conditions set within the simulation. As a result of this validation and benchmark procedure, the dynamic behaviour of each type of thermal box was evaluated, measuring the ramps of internal temperature growth over time as a function of the ISR, as well as the temperature decrease once the radiation source was removed.

Numerous thermal box constructions were built, each featuring different characteristics: presence/absence of thermal insulation around the box (3 cm); internal surface being reflective or black painted. Each thermal box was characterised by the following dimensions: 75x110x200 mm and was subject to the same range of temperatures and radiations.

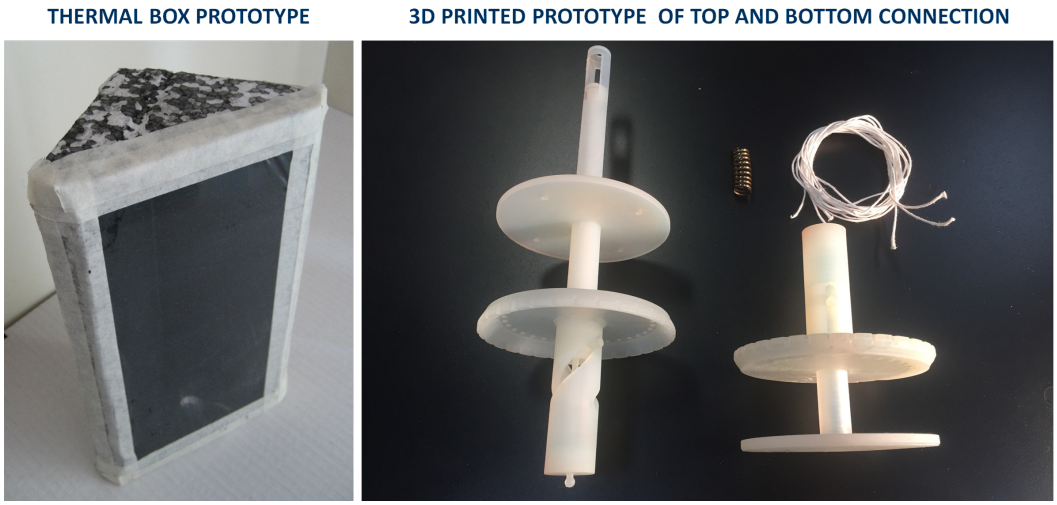

FIG. 10 Prototype of the thermal box, with external insulation and internal black paint [left] and 3D-printed prototype of the top and bottom connections [right]

The prototypes were subjected to radiation with an uncontrolled wavelength spectrum but with a set power. The experimental set-up is presented in Fig. 11.

The standard radiation level was input by means of four light bulbs, each characterised by a power P = 105 W. The light bulbs produced a light distribution that covers the thermal box in a quasi-homogeneous fashion. The thermal box was placed on a wooden board with a rectangular hole so that the lateral sides of the box were not subject to radiation. By vertically sliding the board on different steps, the radiation level at each height was measured by a radiometer. The shorter the distance between the prototype and the lamps, the higher the radiation levels recorded. The relation between the distance and the measured radiation level was then obtained through different

attempts. In fact, indoor thermal box temperature data were collected for an imposed radiation range of 250 to 650 W/m^2, with intermediate steps of 300, 350, 450 and 550 W/m^2. These were deemed suitable considering a typical application (considering the application on a vertical façade, situated in a Mediterranean region).

Each sample was equipped with 2 thermal sensors (thermocouples), glued with conductive adhesive paste on the internal surfaces of the box, one on the top side and another on the bottom side, and all the holes of the thermal box prototype were sealed to avoid air leakage.

The internal temperature was only due to surface temperatures, but the heat exchange mode influenced how fast the internal temperature increases and decreases.

The light bulbs were kept until the two measured surface temperatures stabilises, which means that from a transient scenario, a quasi-stationary heat flow was achieved, and temperature is asymptotic to a value (i.e. they can be considered stationary). In fact, temperature could rise more if the bulbs are left on; however, in reality, a higher temperature rise is balanced by external factors, such as wind and temporary external shading, therefore it was considered conservatively that the maximum reachable temperature should be estimated without letting it rise in a situation that is too constrained.

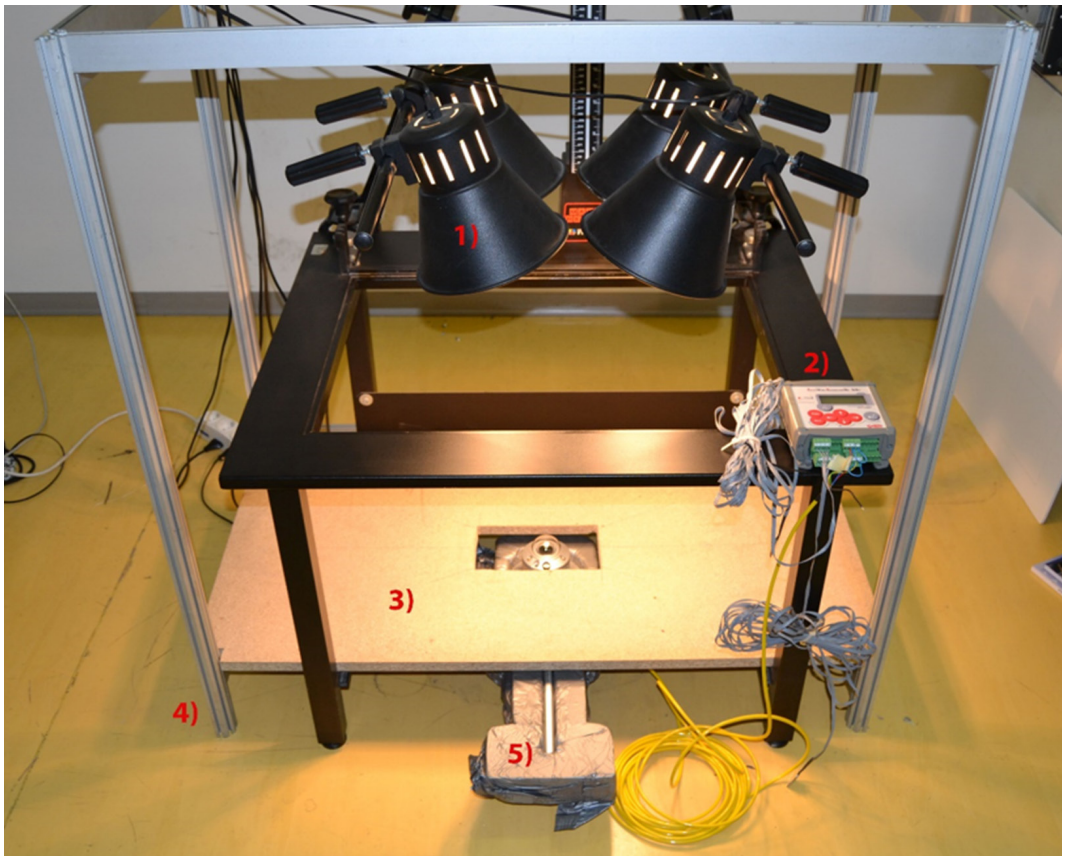

FIG. 11 Test bench: [1] Light bulbs, [2] Data Logger, [3] Timber board, [4] Reference frame [5] pyranometer

Temperatures measured by the thermocouples were registered by a data logger, which measures with a time step of 10 seconds. Therefore, every ten seconds, maximum temperature, minimum temperature, and average temperature are determined and recorded.

4 RESULTS

The experimental findings are summarised within this section. Firstly, the correlation between variable incident solar radiation (ISR) and the temperature inside the thermal box (T_{box}) is shown. A further explanation of the results, in the context of variable external air temperatures (T_{air}) and ISR levels, is given in Section 4.2. Finally, considerations on the target activation temperature (T_{SM}) for a thermal box hosting a SMA spring actuator are presented in Section 4.3.

4.1 CORRELATION BETWEEN ISR AND T_{BOX}

The system was designed to reach a target activation temperature during a time span lower than 50 minutes and under a minimum level of ISR identified in 300 W/m^2. In Fig. 12 an explanatory diagram of temperature distribution is presented for a higher amount of available irradiance equal to 550 W/m^2. The slope describing the increase of the temperature ramp is therefore related to the amount of available ISR. The higher the amount of ISR, the shorter the time interval required to reach the target temperature. In the case of permanent solar radiation level T_{SM} increases until a stationary, balanced temperature (approximated to be equal to a quasi steady-state condition) is reached. Additionally, in this case, the maximum asymptotic temperature reached is related to the value of the imposed radiation and the balance within the thermal losses of the thermal box with the surroundings. When the radiation source is removed, the system returns to the initial conditions in half of the time, on average, that was necessary to reach the maximum registered temperature, suggesting a faster heat dissipation in comparison to the heat build-up process.

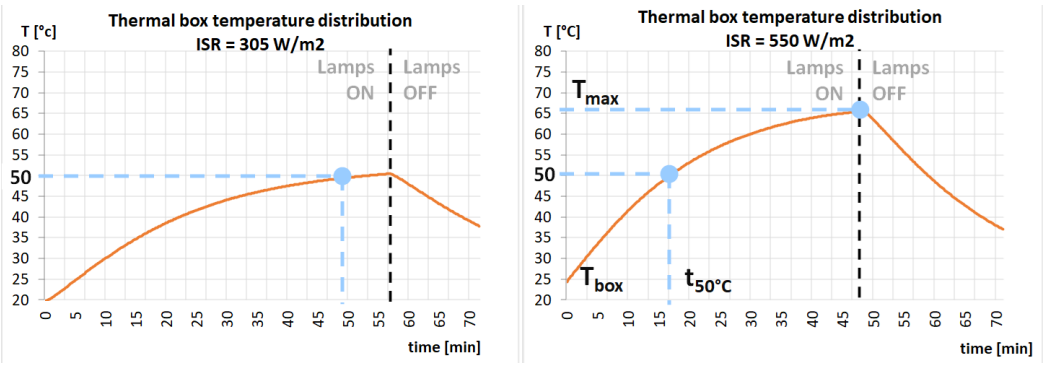

FIG. 12 Relation between temperature increase in the thermal box and exposure time to a radiant source at ISR = 305W/m^2 [left] and 550 W/m^2 [right]

It is therefore possible to assume that with the same air temperature of the surrounding environment as the value of ISR incident on the surface increases, the time for which the activation of the actuator system takes place is drastically reduced. This phenomenon, however, leads to an

increase in the peak temperature reached inside the thermal box, compared to the values obtained with lower ISR. This also leads to an increase in the time for effective cooling (phase delay) and return to optimal neutral, pre-activation temperature conditions.

4.2 DEFINITION OF T_{SM}

On any orientation, the hours of solar radiation higher than 200 W/m^2 are lower than 30% of the total hours of the whole day (night included), which is approximately 50% of the total hours of daylight on a summer's day. The shadings are designed to self-activate when direct solar radiation on the façade surface > 300 W/m^2; however, while the ISR is below 300 W/m^2 but still above 200 W/m^2, the internal temperature of the black box might still be above the activation threshold, avoiding the deployment of shading. The duration of the transition period was then estimated for different orientations, and it was found to be lower than one hour most of the time, which is the minimum time required to reach transition temperature. Fig. 13, presented as an illustrative example of the possible path, shows an explanatory result for a single day analysis cantered on April 26th for a south-oriented façade. If hourly average values of ISR for temperature increase are considered, it is possible to observe that threshold values for ISR are sufficient to allow the system to be activated effectively in a significant range around the central hours of the day, enabling the activation of the shading system for the hours that are considered critical during the day. In addition, there are some low peaks (1 pm), probably due to temporary cloudy weather, during which, even if solar radiation is below 300 W/m^2, shading devices are still activated ("closed").

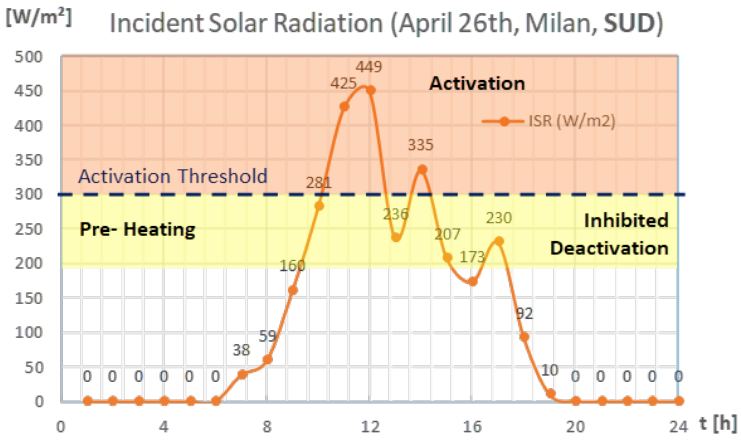

FIG. 13 Radiation Path and activation profile of the system

Whenever the temperature in the thermal box remains slightly above the activation threshold, the system is in an intermediate configuration between "open" and "closed". Whenever an external factor, such as a sudden change in ISR prevents the activation temperature from being achieved (e.g. clouds, obstructions, etc.), the shading device would remain in its intermediate position, waiting for the temperature to rise (when the shading would close) or to go down (when the shading would open). In either case, even when the shadings are not fully closed, they contribute somehow to lower the g-value of the façade system.

In a realistic scenario, the internal temperature is influenced by other factors, and the most important of those, after solar radiation, is external air temperature. When direct solar radiation hits the façade, it is expected that the air temperature inside the box is:

- higher than summer exterior temperature, so that the SMA activation occurs during direct solar presence, and not also during normal hot days with an overcast sky;
- equal to SMA activation temperature during the winter considering direct solar radiation exposition.

With regard to the semi-stationary model discussed in Section 3.1, it is possible to select for example a characteristic day (July 18th) on which the contribution of the incident solar irradiance is strongly effective in raising the temperature inside the Thermal Box (T_{box}), reaching a maximum peak temperature of almost 70°C. Fig. 14 shows that, in accordance with the selected thresholds, an external air temperature of 25°C combined with an irradiance value equal to or higher than 300 W/m^2 can lead to temperature values inside the thermal box of almost 50°C. Therefore, a preliminary assessment may be made considering 50°C as activation temperature (T_{SM}) of the SMA spring, in order to comply with the pre-defined limits as summer thermal comfort descriptors.

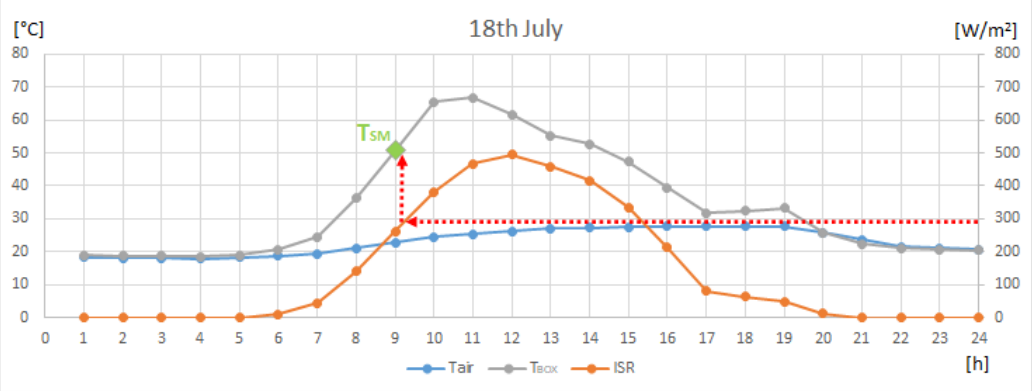

FIG. 14 Effect of solar irradiance on the temperature rise of the thermal box and definition of the activation threshold of the SMA spring element)

4.3 CONSIDERATIONS ON THE ACTIVATION THRESHOLD

The question that arises spontaneously, however, and to which it is necessary to answer is how much the choice of such an activation threshold temperature for the SMA spring is optimal in optimising the passive adaptive behaviour of the shading system.

The carpet diagram presented in Fig. 15 shows the activation profile of the shading system (hours in red) for an activation temperature inside the thermal box (T_{SM}) of 50°C. A similar activation profile is reported in Fig. 16 for T_{SM} = 35°C. It is immediately understood that, as the set-point temperature decreases, there is an increase in the hours in which this activation process would take place. The increase in terms of system working hours is flat and over both winter and summer periods. However, a conservative approach, which could lead to a low set-point temperature, is likely to significantly increase the number of hours of operation, resulting in an almost constant (and potentially unwanted) activation of the system. The choice, instead, of a higher set-up activation temperature, allows the events to be located only in correspondence with the most well known

summer critical periods, by means of effectively controlling and reducing the incident solar radiation over the glazed surfaces. On the other hand, during the winter hours, in which the solar radiation on vertical surfaces is severe, the system can be effective in mitigating daylight issues due to direct glare phenomena.

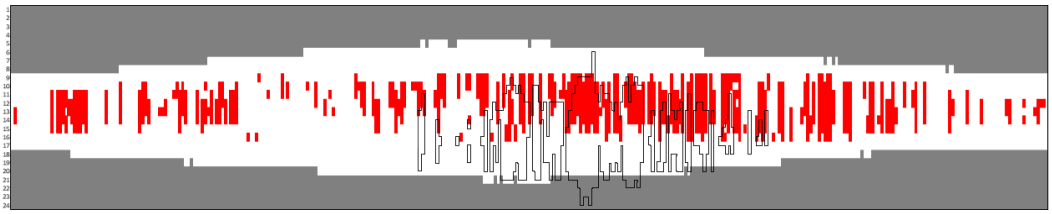

FIG. 15 Annual distribution diagram of system activation hours in SMA depending on SMA spring activation temperatures (TSM). In red the activation hours, in white the remaining daytime hours, and in grey the night-time hours. Distribution for TSM = 50°C

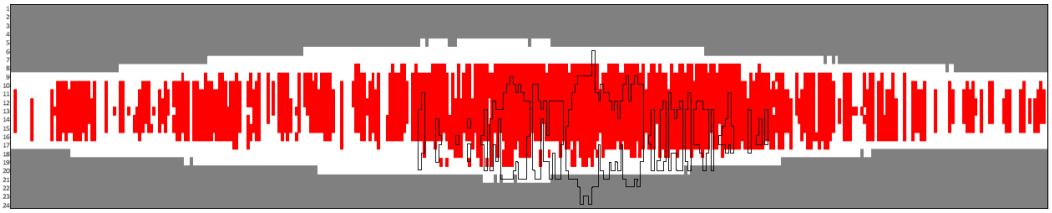

FIG. 16 Annual distribution diagram of system activation hours in SMA depending on SMA spring activation temperatures (TSM). In red the activation hours, in white the remaining daytime hours, and in grey the night-time hours. Distribution for TSM = 35°C

It is worth noting that, based on this case study, activation temperatures (T_{SM}) below 50°C are not desirable, as they do not comply with the requirements set as part as the SMA spring definition process (refer to Chapter 2.2). Furthermore, considering standard classes of SMA springs, those with an activation temperature of 50°C or higher are typically characterised by more favourable stresses and elongation ratios (Otsuka & Ren, 2005). Finally, as explained above, the temperature inside the thermal box (T_{box}) is also influenced by the external air temperature (T_{air}); therefore, a higher T_{SM} will limit the influence of T_{air} on the activation of the shading.

5 CONCLUSIONS

The search for complex shapes and façade kinematics is associated with the concept of responsive building, characterised by complex façade systems using traditional sensor-motor actuation system. Within this context, the authors aimed to describe a workflow to provide an alternative actuation mechanism and a shading geometry, which are compatible with an adaptive passive activation process. The development of the actuators was focussed on SMA materials which could be activated by a localised temperature variation, induced by an external stimulus.

Due to the high number of varying parameters within the simulation and experiments, it was necessary to narrow down the context of the application into a specific case study, to accurately model and assess the functioning and efficacy of the system.

As outlined within Chapter 3, the context considered was a vertical façade, south-oriented, within a building situated in the Mediterranean region, specifically sourcing the environmental data (temperature, solar radiation) from Milan (Italy). This specific location was chosen as it is familiar to the authors, as well as being a good example of a humid subtropical climate (Cfa, according to the Koppen-Geiger classification), with relatively moderate external air temperatures and high levels of incident solar radiation. Within this context, a set of external air temperatures, solar irradiance values and hours of permanence of such conditions were identified, and a SMA component was tailored for the optimised functioning of the shading device.

Once the geometry of the actuator and its required force and type of displacement was defined, the analysis delved into the relationship between the optimal activation temperature and the contextual application, i.e. the expected weather scenario and its climatic variability.

It is noted that, within the commercially available SMA components, the industry is capable of manufacturing SMA springs with a wide range of characteristics: for example, given a required displacement and forces, SMA springs can be developed with different activation temperatures, depending on the desired final requirements. This is achieved by tweaking the manufacturing process, geometrical features and/or alloy composition.

The choice of enclosing the actuation system inside a thermal box allows the activation temperature of the system to be characterised, whilst maximising the effect of the incident solar radiation (ISR) for its operation. It also improves the reactivity of the system actuation by intervening on the rate of change of the indoor temperatures, thus extending the frequency of activation cycles. The temperature inside the thermal box (T_{box}) becomes a representative index in defining the activation (and deactivation) thresholds of the system: determining the optimal value for T_{box} means capturing the effects of a change in air temperature (T_{air}) as well as the effect of incident solar radiation (ISR) over a façade surface.

Once the maximum ISR set-point value for the desired activation was defined, it was possible to estimate the frequency distribution of T_{box} in accordance with the other outdoor weather variables.

From the simulations and experiments carried out by the authors, it is possible to conclude that:

- By means of manipulating the properties of the SMA spring and/or the thermal box, it is possible to programme the activation of these systems in accordance with a set threshold value for ISR, thus allowing activation in different seasons. The number of hours during which the system is capable of matching the imposed set point conditions also depends on the SMA activation temperature (T_{SM}): the lower T_{SM}, the more sensitive the system becomes, resulting in higher frequency of activation, which may cause the system to activate most of the time during the year.
- The system does not adapt to all climates and orientations, and it requires a detailed design for each selected scenario. The authors defined a methodology to determine the number of activation occurrences, and therefore the optimal activation temperature of the SMA component given a specific context.
- The effect of T_{air} can interfere with ISR in raising (or lowering) the value of T_{box} above (or below) the T_{SM} threshold. This is particularly critical in those contexts that are characterised by high external temperatures and/or low solar irradiance. Such conditions could be an east-oriented SMA activated shading during a sunny afternoon, or any application during a hot but cloudy day. In this respect, manual override and/or BMS (building management system) may be considered to regulate unwanted or missed activation of the shading system.
- A static thermal simulation is deemed accurate enough to predict the maximum value for T_{box} reached by the system, as well as to define the geometry of the thermal box, its radiative properties, and its degree of thermal insulation.
- The field measurement on a physical prototype, in conjunction with dynamic analyses, is useful to verify the variation rate over time (both increase and decrease) of T_{box} and T_{air}, by capturing the effect of significant site-related variables (wind speed, cast shading, etc.) besides statistical data for ISR.
- Improving the thermal insulation of the thermal box speeds up the activation process, enhancing the temperature build-up to critical values of T_{box}; at the same time, however, excessive values of T_{box}, if not compensated by natural or forced ventilation within the cavity, may result in prolonged activation (due to increased thermal inertia of the system), even when the system is no longer subject to target levels of ISR.
- Regarding the materiality of the twisting cylinders, the elasticity (or stiffness) of the longitudinal fibres will affect the required strength of the SMA spring, which would have an impact on the required activation stimulus (e.g. the activation temperature).

Acknowledgements

We gratefully thank the members of SEEDlab.abc @Politecnico di Milano (www.seed.polimi.it) for their support during the measurement activities and all the suggestions provided during the writing of the paper. We also thank Pa&Co architecture (http://pacoarchitecture.com/) for their support during the prototyping processes.

References

Coelho, M., & Maes, M. (2009). Shutters : A Permeable Surface for Environmental Control and Communication. *Proceedings of Tangible and Embedded Interaction (TEI '09),* 13-18. https://doi.org/10.1145/1517664.1517671

Coelho, M., & Zigelbaum, J. (2011). Shape-changing interfaces. *Personal and Ubiquitous Computing, 15,* 161-173. https://doi.org/10.1007/s00779-010-0311-y

Decker, M., & Yeadon, P. (2010). SmartScreen: Controlling Solar Heat Gain with Shape Memory Systems. Decker Yeadon LLC. https://archinect.com/news/article/88265/smart-materials-move-smartscreen

Fiorito, F., Sauchelli, M., Arroyo, D., Pesenti, M., Imperadori, M., Masera, G., & Ranzi, G. (2016). Shape Morphing Solar Shadings: A Review. *Renewable and Sustainable Energy Reviews, 55,* 863-884. https://doi.org/10.1016/j.rser.2015.10.086

Gonzalez, N. (2015). Self-Adaptive Membrane. Retrieved from http://www.iaacblog.com/programs/self-adaptive-membrane-_-a-passive-kinetic-system/.

Heschong, L. (2002). Daylighting and Human Performance. *ASHRAE Journal, 44(6),* 65-67.

LIFT Architects (2015). The air flower. Retrieved from http://www.liftarchitects.com/air-flower.

Luna, I. (2014). Shape Memory Alloy responsive façade. Retrieved from http://www.behance.net/gallery/SMAShape-Memory-Alloy/10797251.

Mainini, A.G., Speroni, A., & Vercesi, L. (2018). System for shielding and controlling sun light or the light flow coming from artificial sources, especially for application to buildings. Patent n° WO2018116102-A1.

Mazzucchelli, E. S., Romano, R., Aelenei, L., & Gomes, M.G. (2018). *Passive Adaptive Façades – Examples from COST TU1403 Working Group 1.* Delft, NL: TU Delft Open.

Menzies, G. F., & Wherrett, J. R. (2005). Windows in the workplace: examining issues of environmental sustainability and occupant comfort in the selection of multi-glazed windows. *Energy and Buildings, 37(6),* 623-630. https://doi.org/10.1016/j.enbuild.2004.09.012

Nielsen, M. V., Svendsen, S., & Jensen, L. B. (2011). Quantifying the potential of automated dynamic solar shading in office buildings through integrated simulations of energy and daylight. *Solar Energy, 85(5),* 757-768. https://doi.org/10.1016/j.solener.2011.01.010

Orangevoid (2007). Pixel skin interactive façade. Retrieved from http://fachadasmediales.blogspot.com/2007/12/pixel-skin-interactive-façade.html

Otsuka, K., & Ren, X. (2005). Physical Metallurgy of Ti–Ni-Based Shape Memory Alloys. *Progress in Materials Science, 50(5),* 511-678, https://doi.org/10.1016/j.pmatsci.2004.10.001.

Palmero-Marrero, A. I., & Oliveira, A. C. (2010). Effect of louver shading devices on building energy requirements. *Applied Energy, 87(6),* 2040-2049. https://doi.org/10.1016/j.apenergy.2009.11.020

Sandoval, J. (2012). Gill_Project performance. Retrieved from http://www.youtube.com/watch?v=-X_KxijpJT0.

Tzempelikos, A., & Athienitis, A. K. (2007). The impact of shading design and control on building cooling and lighting demand. *Solar Energy, vol. 81(3),* 369-382. https://doi.org/10.1016/j.solener.2006.06.015

Verma, S. (2016). Adaptive Skin. Retrieved from http://www.designboom.com/project/adaptive-skins-2/ .

Wang, F., Pichatwatana, K., Roaf, S., Zhao, L. Zhu, Z., & Li, J. (2014). Developing a weather responsive internal shading system for atrium spaces of a commercial building in tropical climates. *Building and Environment, 71,* 259-274. https://doi.org/10.1016/j.buildenv.2013.10.003